

Amorphous magnesium silicate ultrasound-assisted precipitation in a mixing system: Population balance modelling and crystallization rates identification

Marie Dietemann, Fabien Baillon, Fabienne Espitalier, Rachel Calvet, Mike Greenhill-Hooper

▶ **To cite this version:**

Marie Dietemann, Fabien Baillon, Fabienne Espitalier, Rachel Calvet, Mike Greenhill-Hooper. Amorphous magnesium silicate ultrasound-assisted precipitation in a mixing system: Population balance modelling and crystallization rates identification. Powder Technology, 2019, 356, pp.83-96. 10.1016/j.powtec.2019.08.004 . hal-02267199

HAL Id: hal-02267199

https://imt-mines-albi.hal.science/hal-02267199

Submitted on 2 Sep 2019

HAL is a multi-disciplinary open access archive for the deposit and dissemination of scientific research documents, whether they are published or not. The documents may come from teaching and research institutions in France or abroad, or from public or private research centers.

L'archive ouverte pluridisciplinaire **HAL**, est destinée au dépôt et à la diffusion de documents scientifiques de niveau recherche, publiés ou non, émanant des établissements d'enseignement et de recherche français ou étrangers, des laboratoires publics ou privés.

Amorphous magnesium silicate ultrasound-assisted precipitation in a mixing system: Population balance modelling and crystallization rates identification

Marie Dietemann [a], Fabien Baillon [a], Fabienne Espitalier [a,*], Rachel Calvet [a], Mike Greenhill-Hooper [b]

[a] Université de Toulouse, IMT Mines d'Albi, UMR CNRS, Centre RAPSODEE, Campus Jarlard, F-81013 Albi, France
[b] Imerys Talc, 2 Place E. Bouillères, 31036 Toulouse, France

Keywords:
Population balance
Precipitation
Magnesium silicate
Ultrasound
Crystallization rates

A B S T R A C T

Natural talc is a very interesting filler for plastic and rubber materials and paints because it enables polymer matrix properties to be improved. Nano-sized particles are required to get a good dispersion of the solid in the polymer matrix. However, at the moment the main drawback in the use of natural talc is that, with a conventional milling process, nanometric particle sizes are difficult and expensive to obtain. A process of magnesium silicate synthesis made by ultrasound-assisted precipitation has been developed in two steps. The first step consists of the synthesis of amorphous magnesium silicate by precipitation from sodium metasilicate and acid magnesium chloride. In the second step, the amorphous solid is transformed in a crystalline solid under pressure. In this study an ultrasound-assisted synthesis of amorphous magnesium silicate is proposed. Some process parameters (ultrasound power, initial reactants molalities and reactants flow rate) have effects on the particle-size distribution. The population balance is modelled and solved by moments method in the steady state to identify nucleation and growth rates and agglomeration kernel as a function of operating conditions and to understand how these conditions affect the particle-size distribution.

1. Introduction

Natural talc is an interesting material that can be used as high performance filler in polymers. Polymers properties, for instance mechanical reinforcement and barrier effects, are improved Ciesielczyk et al. [5]. Talc is used in rubbers in order to improve lubricating properties Tufar [17]. Tensile and transverse strength and the modulus of elasticity of plastics are improved by talc Tufar [17]. This solid also enables to improve the resistance to corrosion of paints, change their flow properties, make spreading easier and reinforce covering power Martin [12]. However, a homogeneous dispersion of the filler in the polymer matrix is necessary to obtain these different performances. A good dispersion in a polymer matrix requires, in an ideal case, particles to be nano-sized Martin et al. [13]. However, obtaining nanometric particles using conventional milling processes is expensive because of an important energetic consumption. An alternative method to milling is the chemical synthesis of talc. This synthesis is made up of two steps. The first step consists of magnesium silicate precipitation with the production of an amorphous solid. A second step is necessary to convert the amorphous solid into crystalline lamellar nano-sized particles with a talc-like structure. Amorphous and crystalline forms of magnesium silicate can be used, depending on the industrial application.

The first step of the process of producing amorphous magnesium silicate has been studied by Dietemann et al. [6]. The aim of this work was to study the influence of precipitation parameters on product properties. Effects of some process parameters, such as reactant molalities, temperature and the mixing system used with an ultrasound probe, on the properties of amorphous magnesium silicate, in particular on the particle-size distribution, have been studied.

However effects of these process parameters on crystallization rates (nucleation rate, growth rate and agglomeration kernel) haven't been studied. The knowledge of these effects would enable to understand process parameters effects on the particle-size distribution and how these process parameters affect crystallization rates. The aim of this paper is to identify crystallization rates as a function of process parameters with use of ultrasound and understanding the ultrasound-assisted precipitation phenomena in order to control the particle size of solid.

2. Experimental section

2.1. Materials

The amorphous magnesium silicate was synthesized by a precipitation between a sodium metasilicate solution (Na_2SiO_3, $5H_2O$) and an

* Corresponding author.
E-mail address: Fabienne.Espitalier@mines-albi.fr (F. Espitalier).

acid magnesium chloride solution ($MgCl_2$, $6H_2O$), according to the following equation Martin et al. [13]:

$$4Na_2SiO_3, 5H_2O + 3MgCl_2, 6H_2O + 2HCl = Si_4Mg_3O_{11}, 5H_2O + 8NaCl + 34H_2O$$

The reactants were aqueous solutions of sodium metasilicate (purity 95%), and of magnesium chloride (purity 99%), (supplier Prolabo). The initial molar ratio Mg/Si was always 0.750.65, corresponding to that of natural talc. Hydrochloric acid 1 M was added to the aqueous solution of magnesium chloride (supplier Prolabo). Demineralised water was used. The water moles number in the magnesium silicate solid has been estimated by the solid weight loss at 550 °C [6]. This value, $n = 5$, has been confirmed by Dynamic Vapour Sorption analysis.

2.2. Procedures and methods

2.2.1. Synthesis of magnesium silicate

To ensure proper mixing of the reactants and optimal application of ultrasound, a small volume cell adapted to our probe was chosen to do the precipitation [1]. The precipitation occurred in aThe characteristic of the mixing system (Fig. 1) are: diameter D = 4 cm, height H = 6 cm and volume 42 mL. Peristaltic pumps were used to feed solutions into the mixing system.

The following operating conditions are studied at different values:

- reactants molalities

([$MgCl_2$, $6H_2O$] = 0.52, 0.73, 1.03, 1.26, 1.47, 2.21 and 2.94 mol·kg^{-1}; [Na_2SiO_3, $5H_2O$] = 0.50, 0.71, 1.00, 1.22, 1.43, 2.14 and 2.86 mol·kg^{-1}); ([HCl] = 0.35, 0.50, 0.72, 0.87, 1.00, 1.50 and 2.00 mol·kg^{-1}).

- reactants flow rate (Q_M = 128.4, 205.0 and 328.3 g·min^{-1}). The partial flowrates [$MgCl_2$]/[Na_2SiO_3] are 50/78 g·min^{-1}, 80/125 g·min^{-1} and 128/201 g·min^{-1} for a total flowrate Q_M of respectively 128.4, 205.0 and 328.3 g·min^{-1}.

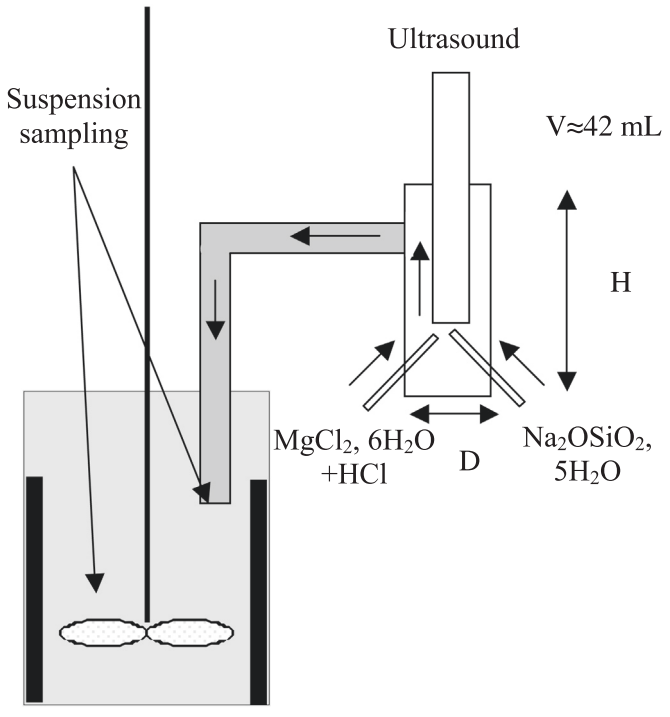


Fig. 1. Experimental device of the precipitation process.

- and ultrasound power P_{US} (0.0, 34.5 and 70.6 W at 20 kHz) during the precipitation in the mixing system.

The Table 1 gives the operating conditions of each experiments.

The ultrasound power dissipation in the solution was measured by the calorimetry method.

At the exit of the mixing system, the suspension was poured into a vessel which was initially filled with 100 mL of demineralised water. This vessel was equipped with four baffles and stirred. The mixing device was a PTFE helix propeller with four squared blades. Its diameter was 4 cm. The stirring rate was 600 rpm. The total volume of the suspension was 1 L.

In a previous work, Dietemann et al. [6] showed amorphous silica could precipitate with amorphous magnesium silicate. This co-precipitation occured if an excess of hydrochloric acid was used in initial reactants molalities.

2.2.2. Evaluation of the properties of synthetic magnesium silicate

Suspension and solid were submitted for physico-chemical properties evaluation.

2.2.2.1. Particule-size distribution. Samples were taken of the suspension to be analysed by the dynamic light scattering technique using a Malvern Mastersizer 2000. This enables particle-size distribution to be followed during the synthesis. The suspension was diluted with water in the cell of the granulometer. Ultrasound (about 3 mW) was applied during 2 min before the size measurement following established protocol showed by Dietemann et al. [6]. Samples were taken of the suspension in two different points (Fig. 1): at the exit of the mixing system or at the exit of the tube that enabled the suspension to flow inside the vessel.

2.2.2.2. pH of the suspension. The pH and the temperature of the suspension were measured at the exit of the mixing system.

2.2.2.3. Chemical composition of solid. Analyses by X-Ray fluorescence spectrometry were used to calculate Mg/Si ratio in the synthesized solid that had been washed, dried and milled as it is explained by Dietemann et al. [6]. The solid powder was then mixed with lithium meta and tetra-borate. A pearl was formed from this mixture in the apparatus Perlix'3. A Philips (WD-XRF) - PW2504 apparatus was used for these analyses. It was a wavelength-dispersive apparatus.

3. Chemical equilibrium calculations and precipitation process

3.1. Chemical equilibrium calculations involved during the precipitation reaction

The objective of the resolution of the chemical equilibrium calculations is to determine supersaturation ratio of amorphous magnesium

Table 1
Operating conditions and process parameters.

Experiment	[$MgCl_2$, $6H_2O$] (mol·kg^{-1})	[Na_2SiO_3, $5H_2O$] (mol·kg^{-1})	[HCl] (mol·kg^{-1})	T (°C)	P_{US} (W)	Q_M (g·min^{-1})
1	0.52	0.50	0.35	20.0	0.0	205.0
2	0.73	0.71	0.50	20.0	0.0	205.0
3	1.03	1.00	0.72	20.0	0.0	205.0
4	1.26	1.22	0.87	20.0	0.0	205.0
5	0.73	0.71	0.50	20.0	34.5	205.0
6	1.47	1.43	1.00	20.0	34.5	205.0
7	2.21	2.14	1.50	20.0	34.5	205.0
8	2.94	2.86	2.00	20.0	34.5	205.0
9	0.73	0.71	1.00	20.0	0.0	205.0
10	0.73	0.71	1.00	20.0	34.5	205.0
11	0.73	0.71	1.00	20.0	70.6	205.0
12	0.73	0.71	1.00	20.0	70.6	328.3
13	0.73	0.71	1.00	20.0	70.6	128.4

Table 2
Chemical equilibria, associated K constants and solubility products K_s (* phreeqc.dat database of PHREEQC software, [4]).

Chemical equilibrium	K equilibrium constant	log(K) *
$(Si_4Mg_3O_{11}, 5H_2O)_{solide} + 6H^+ = 3Mg^{2+} + 4H_4SiO_4$	$K_{s1} = \left(\frac{a^3_{Mg^{2+}} a^4_{H_4SiO_4}}{a_{Si_4Mg_3O_{11},5H_2O} a^6_{H^+}}\right)_{éq}$	Unknown
$(SiO_2)_{solide} + 2H_2O = H_4SiO_4$	$K_{s2} = \left(\frac{a_{H_4SiO_4}}{a^2_{H_2O} a_{SiO_2}}\right)_{éq}$	−3,98
$Mg^{2+} + H_2O = MgOH^+ + H^+$	$K_3 = \left(\frac{a_{H^+} a_{MgOH^+}}{a_{Mg^{2+}} a_{H_2O}}\right)_{éq}$	−11,44
$H_4SiO_4 = H_3SiO_4^- + H^+$	$K_4 = \left(\frac{a_{H^+} a_{H_3SiO_4^-}}{a_{H_4SiO_4}}\right)_{eq}$	$-302{,}3724 - 0{,}050698*T + \frac{15\ 669{,}69}{T} + 108{,}18{,}466*\log(T) - \frac{1\ 119\ 669{,}0}{T^2}$
$H_4SiO_4 = H_2SiO_4^{2-} + 2H^+$	$K_5 = \left(\frac{a^2_{H^+} a_{H_2SiO_4^{2-}}}{a_{H_4SiO_4}}\right)_{eq}$	$-294{,}0184 - 0{,}050698*T + \frac{15\ 669{,}69}{T} + 108{,}18{,}466*\log(T) - \frac{1\ 119\ 669{,}0}{T^2}$
$H_2O = OH^- + H^+$	$K_e = \left(\frac{a_{H^+} a_{OH^-}}{a_{H_2O}}\right)_{eq}$	$-283{,}971 - 0{,}05069842*T + \frac{13\ 323{,}0}{T} + 102{,}24{,}447*\log(T) - \frac{1\ 119\ 669{,}0}{T^2}$

silicate versus operating conditions. The equilibrium calculations were solved using the PHREEQC Charlton and Parkhurst [4] speciation calculation software. The initial molalities of the Na, Mg, Si and Cl species, the initial water mass, the temperature, as well as the equilibrium equation for the formation of magnesium silicate, constitute the input data. The software calculates, in particular, the activity coefficients, the activities and the molalities of the various species present in solution, the initial supersaturations of the magnesium silicate and the silica, as well as the temperature, the pH and the conductivity of the suspension (solution with solids).

The PHREEQC software resolve the following system (see 8) including equations of:

- electroneutrality;
- material balances of some species (Mg, Si, O, H, Na);
- ionic strength of the solution;
- activity of water.

The equilibria involved in the precipitation reaction, which is responsible for the formation of amorphous magnesium silicate $Si_4Mg_3O_{11}$, nH_2O and amorphous silica SiO_2 are presented in the Table 2. Only the main species and their equilibrium are presented in this table. Some species, with a very low molality, are not presented. The species in solution are: OH^-, H^+, H_2O, Cl^-, Mg^{2+}, $MgOH^+$, Na^+, H_4SiO_4, $H_3SiO_4^-$, $H_2SiO_4^{2-}$, SiO_2 and $Si_4Mg_3O_{11}, 5H_2O$.

For each chemical equilibrium, the associated equilibrium constant K or the solubility product K_s is written according to the activities a_i species in solution and its value or expression as a function of the temperature T, if known, are specified. These values or expressions of the equilibrium constant or solubility product are provided by the database of speciation software, PHREEQC [4]. The pH of solution is calculated from the activity of the species H^+ and is given by the following relation (PHREEQC software database):

$$pH = -\log(a_{H^+}) \tag{2}$$

Since the equilibrium constant of amorphous magnesium silicate is not implemented in the PHREEQC software database, it has been identified. The chemical equilibrium for the magnesium silicate has been chosen in agreement with those of talcum available in PHREEQC database. A paper concerning chemical properties of an amorphous magnesium silicate present in detail its determination [6].

The Table 3 presents the models used to calculate the activity coefficient γ_i, depending on the species i considered. For the charged species, the choice of the model depends on the knowledge of the specific parameters of the species, a^0 and b. In cases where these parameters are known, their values are specified in the table.

The values of the ionic strength calculated for the different experiments are between 0.7 and 2.7 mol·kg^{-1}. These values are higher

Table 3
Coefficients of activity of different species in solution (* PHREEQC software database: phreeqc.dat).

Model	Species in solution	Specific parameters *
Debye-Hückel extended equation	H^+	Ion: $a^0 = 0,90$, $b = 0$
I<0,05 mol·kg^{-1}	OH^-	$a^0 = 0,35$; $b = 0$
a^0 and b known	Na^+	$a^0 = 0,40$; $b = 0{,}075$
$\log_{10}(\gamma_i) = \frac{-Az_i^2\sqrt{I}}{1 + Ba^0\sqrt{I}} + bI$	Mg^{2+}	$a^0 = 0,55$; $b = 0{,}200$
	Cl^-	$a^0 = 0,35$; $b = 0{,}015$
Davies extended equation	$MgOH^+$	
I<0,5 mol·kg^{-1}	$H_3SiO_4^-$	–
a^0 and b unknown	$H_2SiO_4^{2-}$	
$\log_{10}(\gamma_i) = -Az_i^2\left(\frac{v\sqrt{I}}{1+\sqrt{I}} - 0,3I\right)$		
Setchenow equation		
I<0,002 mol·kg^{-1}	H_4SiO_4	–
Neutral species		
$\log_{10}(\gamma_i) = 0,1I$		

I, ionic strength of the solution.
z_i, ion charge i.
a^0 and b, specific parameters of the considered ionic species.
A and B, temperature dependent constants given by
$A = 9,37 * 10^{-4} * T + 4,86 * 10^{-1}$ (determined from Bard et al. [2])
$B = 2 * 10^{-3} * T + 3,34$ (determined from Bard et al. [2])

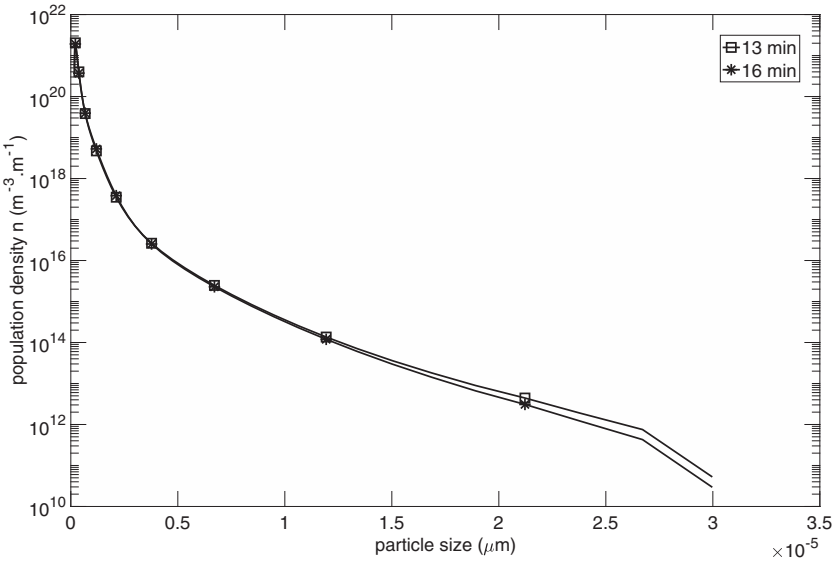


Fig. 2. Number population density in the system 1 ([$MgCl_2$, $6H_2O$] = 0.73 mol·kg^{-1}, [Na_2SiO_3, $5H_2O$] = 0.71 mol·kg^{-1}, [HCl] = 0.50 mol·kg^{-1}, P_{US} = 34.5 W).

than the application ranges of the models presented in the Table 3. Calculation errors probably follow from this.

Amorphous magnesium silicate solubility was estimated from the precipitation using PHREEQC, a computer program for speciation calculations. The equation between the equilibrium constant of amorphous magnesium silicate K_s and the temperature was determined:

$$\log K_s = -0.2399 * T + 108.82 \quad (3)$$

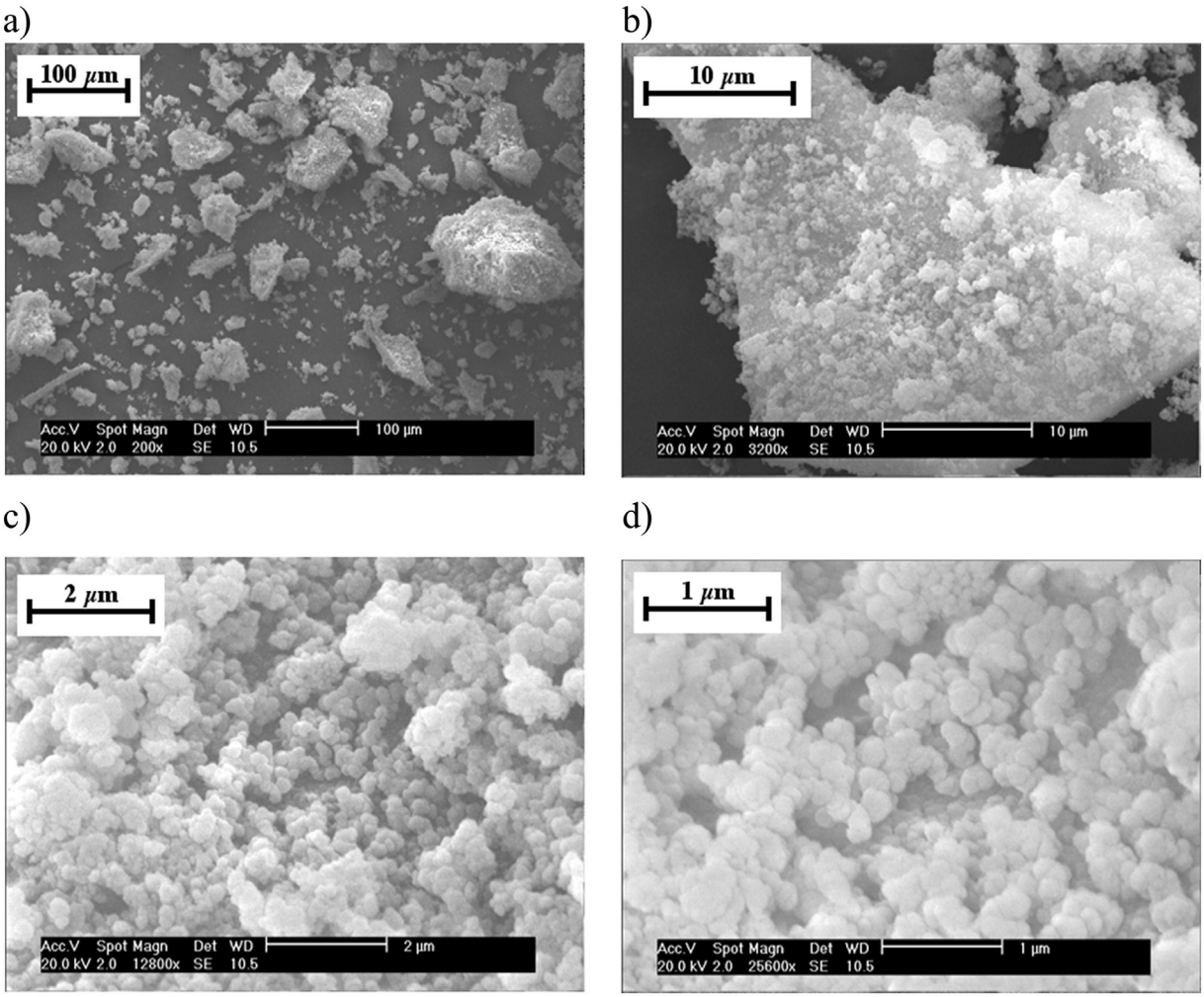


Fig. 3. SEM analyses of amorphous magnesium silicate ([$MgCl_2$, $6H_2O$] = 1.47 mol·kg^{-1}, [Na_2SiO_3, $5H_2O$] = 1.43 mol·kg^{-1}, [HCl] = 1.00 mol·kg^{-1}, T = 20 °C).

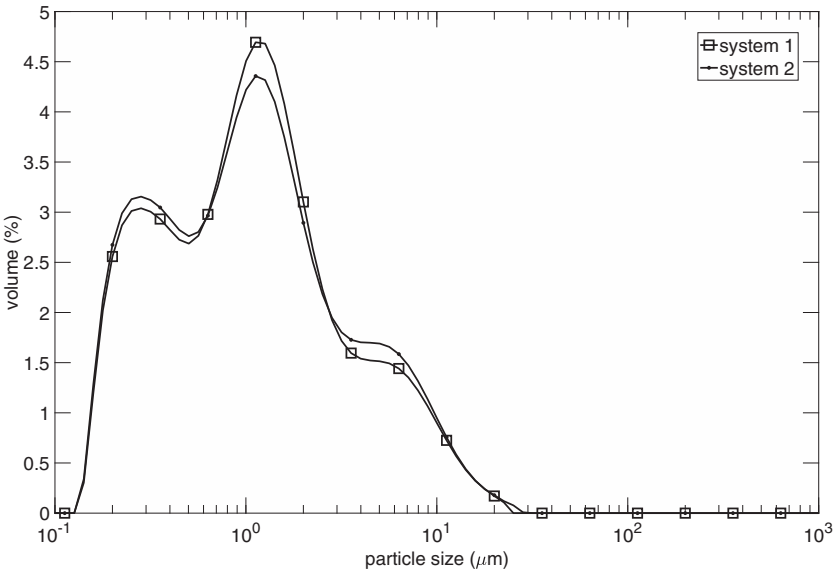


Fig. 4. Particle-size distributions comparison in systems 1 and 2, for the experiment 5 ([$MgCl_2$, $6H_2O$] = 0.73 mol·kg^{-1}, [Na_2SiO_3, $5H_2O$] = 0.71 mol·kg^{-1}, [HCl] = 0.50 mol·kg^{-1}, P_{US} = 34.5 W).

with the chemical equilibrium of amorphous magnesium silicate:

$$(Si_4Mg_3O_{11}, 5H_2O)_{solid} + 6H^+ = 3Mg^{2+} + 4H_4SiO_4 \tag{4}$$

and the equilibrium constant of amorphous magnesium silicate:

$$K_s = \left(\frac{a^3_{Mg^{2+}} a^4_{H_4SiO_4}}{a_{Si_4Mg_3O_{11},5H_2O} a^6_{H^+}} \right)_{eq} \tag{5}$$

The knowledge of the equilibrium constant of amorphous magnesium silicate enables to calculate its supersaturation ratio S:

$$S = \frac{a_{Si_4Mg_3O_{11}} a^5_{H_2O}}{K_s} \tag{6}$$

3.2. Precipitation process

The precipitation process of magnesium silicate and silica is unknown. Chemical equilibria are studied in the mixing system for each experiment in order to see if the precipitation of two solids can occur. Two hypotheses were tested.

3.2.1. Hypothesis 1

Amorphous magnesium silicate alone precipitates. It is assumedsupposed to be supersaturated in the mixing system or in the vessel. Amorphous silica can be supersaturated or undersaturated. Magnesium silicate supersaturation ratio is adjusted to obtain $pH^{calculated} = pH^{experimental}$. The Moles number of magnesium silicate solid is calculated.

3.2.2. Hypothesis 2

Both solids precipitate. Silica is supposed to be at the equilibrium state so its supersaturation ratio is equal to 0. Magnesium silicate supersaturation ratio is adjusted to obtain $pH^{calculated} = pH^{experimental}$. The Moles number of both solids are calculated.

To make these calculations, initial molalities of species Na, Si, Cl and Mg, total mass of water, final temperature of the suspension and chemical equilibria constitute the input data. Chemical equilibria have been previously presented by Dietemann et al. [6]. The program notably calculates activity coefficients, final activities and molalities of different species in solution, the temperature and the pH of the suspension without and with precipitated solid.

4. Population balance modelling

The measurements of residence time distributions have shown that with a medium flowrate without ultrasound or with all flowrates with ultrasound, the mixing system can be considered as perfectly mixed. Measurements of residence time distribution with water were made in silent condition and with ultrasound. We chose as tracer an electrolyte (potassium chloride) dissolved in water at a concentration of 260 g·L^{-1} and we made a negative step. We showed that from medium flow without ultrasound (205 g·min^{-1}) and at all flow rates studied with ultrasound, the mixing system can be considered as perfectly stirred.

The logarithm of the population density of the suspension at the exit of the mixing cell at 13 and 16 min is not linear (Fig. 2). It can be due to the agglomeration phenomenon that can occur during the precipitation process in the mixing system (Fig. 3) or/and to the growth rate that would depend on particles size.

The population balance written with the agglomeration term is given by [16]:

$$\begin{aligned} r_{Nv}\delta(V_p - V_{pc}) - \frac{\partial(G_v n_v)}{\partial V_p} - \frac{Q_s n_v}{V} \\ + \frac{1}{2}\int_0^{V_p} \beta(V_{p1}, V_{p2}) n_v(V_{p1}, t) n_v(V_p - V_{p1}, t) dV_{p1} \\ - n_v(V_p, t) \int_0^{+\infty} \beta(V_{p'}, V_p) n_v(V_{p'}, t) dV_{p'} = 0 \end{aligned} \tag{7}$$

with r_{Nv} the secondary nucleation rate (L^{-1}·s^{-1}), $\delta(V_p - V_{pc})$ the Dirac function, V_p and V_{pc} the volume and the critical volume of a nucleus (m^3), G_v the growth rate (m·s^{-3}), n_v the population density for a class i of volume V_p at time t (L^{-1}·m^{-3}), β, the agglomeration kernel (L·s^{-1}), Q_s suspension volume flows at the exit of the system (L·s^{-1}) and V the mixing system volume (L). $n_v dV_p$ is the number of crystals by suspension volume unit with a volume ranged in $[V_p, V_p + dV_p]$. The population balance is resolved by the moment transformation with respect to volume. The i^{th} order volume moment $m_{v,j}$ is calculated

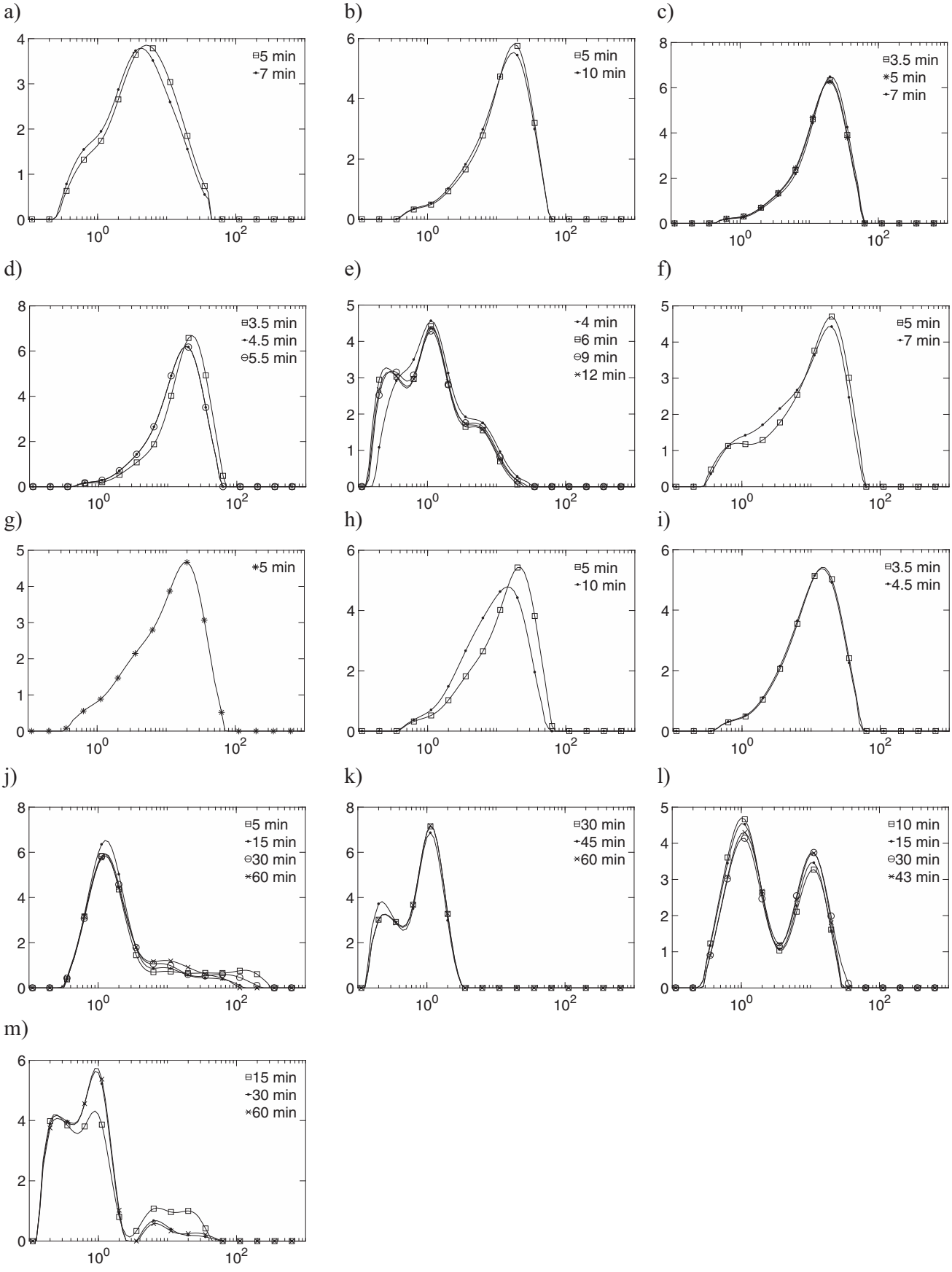


Fig. 5. Temporal particle-size distribution evolution for every experiment.

Table 4
pH, supersaturation ratios at the exit of mixing system and moles numbers calculations (PHREEQC speciation calculations; the kept hypothesis is written in **bold characters**; 1 = magnesium silicate; 2 = silica; a negative moles number means matter must be supplied to form the solid.).

	Hypothesis 1						Hypothesis 2				
Experiment	pH_{exp}	pH_{calc}	$\log(S_1)$	n_1 (mol)	$\log(S_2)$	n_2 (mol)	pH^{calc}	$\log(S_1)$	n_1 (mol)	$\log(S_2)$	n_2 (mol)
1	11.81	**11.81**	**14.59**	$\mathbf{7.472*10^{-2}}$	**−0.38**	**0**					
2	11.63	**11.63**	**14.62**	$\mathbf{1.249*10^{-1}}$	**−0.22**	**0**	11.62	16	$1.070*10^{-1}$	0	$-1.590*10^{-2}$
3	11.55	**11.55**	**11.83**	$\mathbf{2.072*10^{-1}}$	**−0.40**	**0**					
4	10.60	**10.60**	**7.33**	$\mathbf{1.936*10^{-1}}$	**0.07**	**0**					
5	10.06	**10.06**	**3.05**	$\mathbf{1.595*10^{-1}}$	**−0.07**	**0**	10.12	3	$1.592*10^{-1}$	0	$-9.680*10^{-4}$
6	11.26	11.26	15.48	$1.393*10^{-1}$	0.26	0	11.28	14	$1.460*10^{-1}$	0	$1.020*10^{-2}$
7	9.57	**9.57**	**11.31**	$\mathbf{2.250*10^{-1}}$	**1.56**	**0**	9.64	5	$2.305*10^{-1}$	0	$4.570*10^{-2}$
8	11.26	**11.26**	**16.67**	$\mathbf{1.498*10^{-1}}$	**0.38**	**0**	11.20	14	$1.550*10^{-1}$	0	$6.890*10^{-3}$
9	9.15	9.15	8.50	$9.985*10^{-1}$	1.74	0	9.10	1	$1.069*10^{0}$	0	$1.404*10^{0}$
10	9.00	**9.00**	**7.76**	$\mathbf{1.020*10^{0}}$	**1.83**	**0**	8.96	0	$1.070*10^{0}$	0	$1.408*10^{0}$
11	9.03	**9.03**	**8.82**	$\mathbf{1.010*10^{0}}$	**1.80**	**0**	8.97	1	$1.069*10^{0}$	0	$1.408*10^{0}$
12	8.70	**8.70**	**6.49**	$\mathbf{1.042*10^{0}}$	**1.83**	**0**	8.86	0	$1.070*10^{0}$	0	$1.409*10^{0}$
13	9.34	**9.34**	**8.78**	$\mathbf{9.826*10^{-1}}$	**1.85**	**0**	9.31	3	$1.070*10^{0}$	0	$1.410*10^{0}$

Table 5
Amorphous magnesium silicate supersaturation ratio, nucleation and growth rates and agglomeration kernel in the system 2, as a function of process parameters.

Experiment	$[MgCl_2, 6H_2O]$ $(mol\cdot kg^{-1})$	$[Na_2SiO_3, 5H_2O]$ $(mol\cdot kg^{-1})$	$[HCl](mol\cdot kg^{-1})$	T (°C)	P_{US} (W)	Q_M $(g\cdot min^{-1})$	G_v $(m^3\cdot s^{-1})$	β $(L\cdot s^{-1})$	r_{Nv} $(L^{-1}\cdot s^{-1})$	pH	log(S)
1	0.52	0.50	0.35	20.0	0.0	205.0	$4.4*10^{-20}$	$1.3*10^{-11}$	$1.6*10^{15}$	11.81	14.59
2	0.73	0.71	0.50	20.0	0.0	205.0	$4.1*10^{-19}$	$3.8*10^{-11}$	$1.6*10^{14}$	11.63	14.62
3	1.03	1.00	0.72	20.0	0.0	205.0	$8.7*10^{-19}$	$3.2*10^{-11}$	$7.4*10^{13}$	11.55	11.83
4	1.26	1.22	0.87	20.0	0.0	205.0	$9.4*10^{-19}$	$2.2*10^{-11}$	$7.1*10^{13}$	10.60	7.33
5	0.73	0.71	0.50	20.0	34.5	205.0	$2.3*10^{-21}$	$3.2*10^{-13}$	$6.7*10^{16}$	10.06	3.05
6	1.47	1.43	1.00	20.0	34.5	205.0	$7.8*10^{-20}$	$1.7*10^{-11}$	$7.5*10^{15}$	11.26	15.48
7	2.21	2.14	1.50	20.0	34.5	205.0	$2.0*10^{-19}$	$1.6*10^{-11}$	$1.9*10^{15}$	9.57	11.31
8	2.94	2.86	2.00	20.0	34.5	205.0	$3.9*10^{-19}$	$1.0*10^{-11}$	$5.6*10^{14}$	11.26	16.67
9	0.73	0.71	1.00	20.0	0.0	205.0	$4.9*10^{-19}$	$3.4*10^{-11}$	$7.0*10^{13}$	9.15	8.50
10	0.73	0.71	1.00	20.0	34.5	205.0	$4.0*10^{-20}$	$6.0*10^{-10}$	$1.9*10^{17}$	9.00	7.76
11	0.73	0.71	1.00	20.0	70.6	205.0	$1.8*10^{-21}$	$7.5*10^{-15}$	$1.2*10^{15}$	9.03	8.82
12	0.73	0.71	1.00	20.0	70.6	328.3	$4.5*10^{-20}$	$6.5*10^{-12}$	$4.5*10^{15}$	8.70	6.49
13	0.73	0.71	1.00	20.0	70.6	128.4	$9.7*10^{-22}$	$1.7*10^{-12}$	$3.5*10^{17}$	9.34	8.78

Table 6
Nucleation and growth rates and agglomeration kernel in systems 1 and 2 for the experiment 5.

System	$[MgCl_2, 6H_2O](mol\cdot kg^{-1})$	$[Na_2SiO_3, 5H_2O](mol\cdot kg^{-1})$	$[HCl](mol\cdot kg^{-1})$	T (°C)	P_{US} (W)	Q_M $(g\cdot min^{-1})$	G_v $(m^3\cdot s^{-1})$	β $(L\cdot s^{-1})$	r_{Nv} $(L^{-1}\cdot s^{-1})$	pH
1	0.73	0.71	0.50	20.0	34.5	205.0	$3.3*10^{-21}$	$4.8*10^{-13}$	$4.8*10^{-16}$	10.06
2	0.73	0.71	0.50	20.0	34.5	205.0	$2.3*10^{-21}$	$3.2*10^{-13}$	$6.7*10^{-16}$	10.10

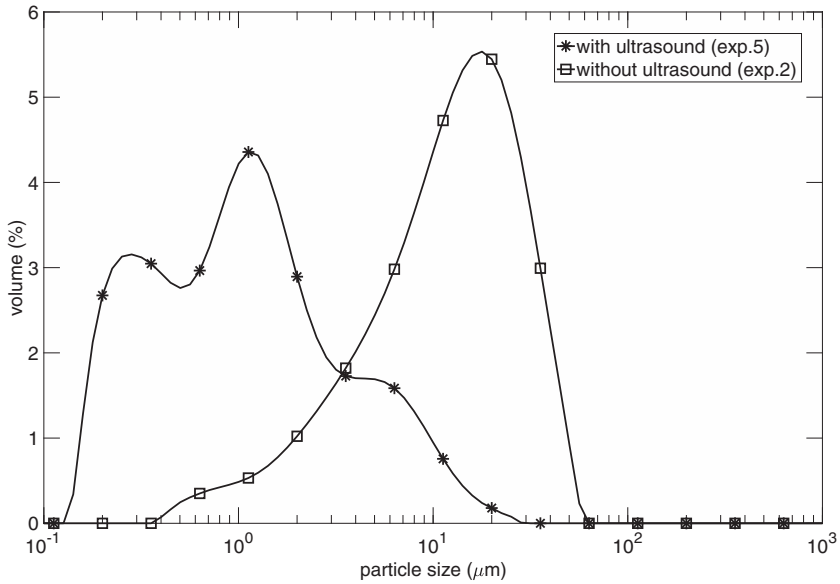


Fig. 6. Effects of ultrasound on the particle-size distribution. ($[MgCl_2, 6H_2O] = 0.73\ mol\cdot kg^{-1}$, $[HCl] = 0.50\ mol\cdot kg^{-1}$)

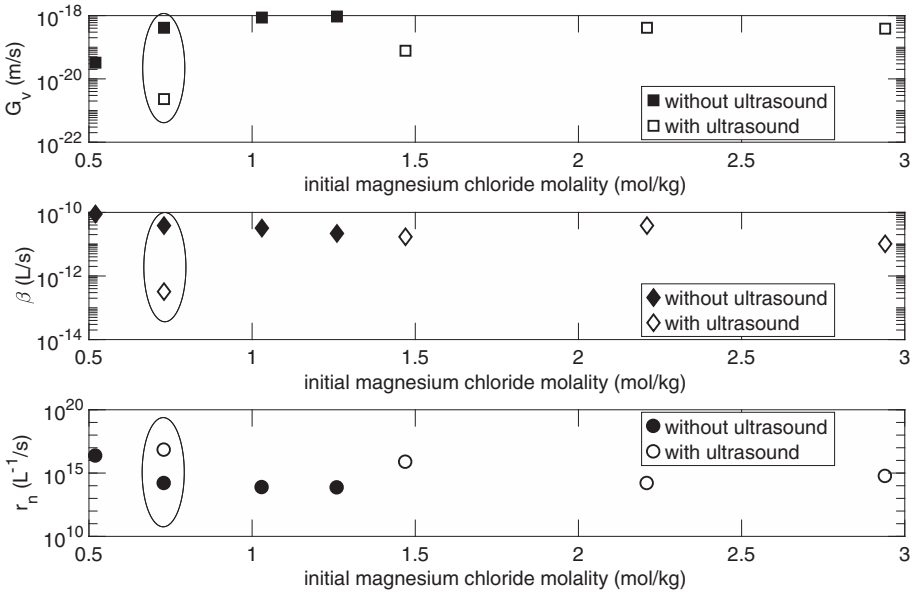


Fig. 7. Nucleation and growth rates and agglomeration kernel versus initial reactants molalities and use of ultrasound.

from the following equation:

$$m_{v,j} = \int_0^{+\infty} V_p^j n_v dV_p \tag{8}$$

The population balance (Eq. (7)) can be written with volume moments. Eq. (7) is multiplied by the term $V_p^j dV_p$ and integrated between 0 and $+\infty$:

$$M_{v,j,agg} + \int_0^{+\infty} r_{Nv}\delta(V_p - V_{pc})V_p^j dV_p - \int_0^{+\infty} \frac{\partial(G_v n_v)}{\partial V_p} V_p^j dV_p - \int_0^{+\infty} \frac{Q_s n_v}{V} V_p^j dV_p = 0 \tag{9}$$

Tavare [16] has showed that Eq. (9) can be written:

$$(0)^j r_{Nv} + G_v j m_{v,j-1} - \frac{Q_s}{V} m_{v,j} + M_{v,j,agg} = 0 \tag{10}$$

According to Hulburt and Katz [11], the k^{th} order volume moment of the agglomeration term is written, in a case of a constant agglomeration kernel β:

$$M_{v,k,agg} = \beta\left[\frac{1}{2}\left(\sum_{j=0}^{k}\binom{k}{j} m_{v,j} m_{v,k-j}\right) - m_{v,0} m_{v,k}\right] \tag{11}$$

with $\binom{k}{j} = \frac{k!}{j!(k-j)!}$ and k = 0, 1, 2, …

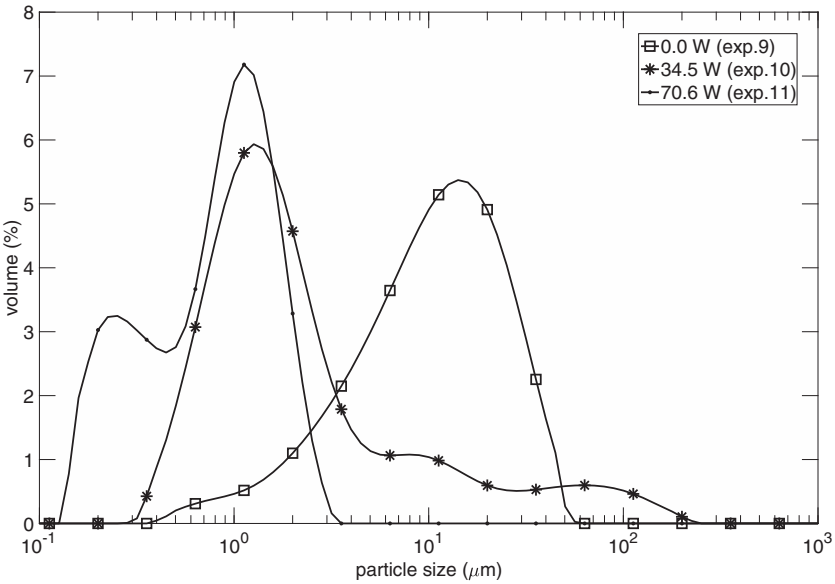


Fig. 8. Effects of ultrasound power on the particle-size distribution. ([$MgCl_2$, $6H_2O$] = 0.73 mol·kg^{-1}, [HCl] = 1.00 mol·kg^{-1})

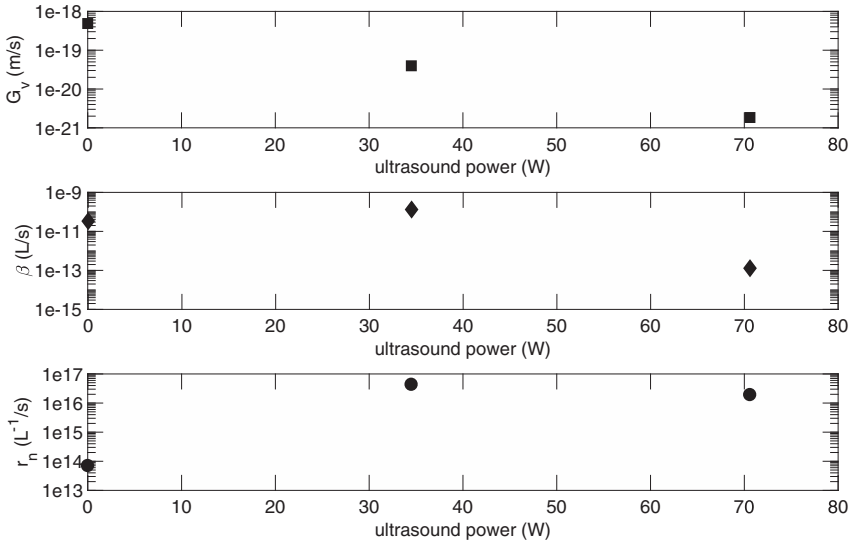


Fig. 9. Nucleation and growth rates and agglomeration kernel versus ultrasound power.

The 0^{th}, 1^{th} and 2^{th} order volume moments are calculated from the last equation (Huburt and Katz [11]):

$$M_{v,0,agg} = -\beta\frac{m_{v,0}^2}{2} \tag{12}$$

$$M_{v,1,agg} = 0 \tag{13}$$

$$M_{v,2,agg} = \beta m_{v,1}^2 \tag{14}$$

Calculations of moments are presented in Appendix 1.

So population balances for the moments of orders 0, 1 and 2 are obtained as:

$$r_{Nv} - \frac{Q_s}{V}m_{v,0} - \beta\frac{m_{v,0}^2}{2} = 0 \tag{15}$$

$$G_v m_{v,0} - \frac{Q_s}{V}m_{v,1} = 0 \tag{16}$$

$$2G_v m_{v,1} - \frac{Q_s}{V}m_{v,2} + \beta m_{v,1}^2 = 0 \tag{17}$$

Eq. (16) enables to calculate G_v:

$$G_v = \frac{m_{v,1}}{\tau m_{v,0}} \tag{18}$$

with $\tau\left(=\frac{V}{Q_s}\right)$ the residence time in the mixing system.

The agglomeration kernel β is determined from Eq. (17):

$$\beta = \frac{-2}{\tau m_{v,0}} + \frac{m_{v,2}}{\tau m_{v,1}^2} \tag{19}$$

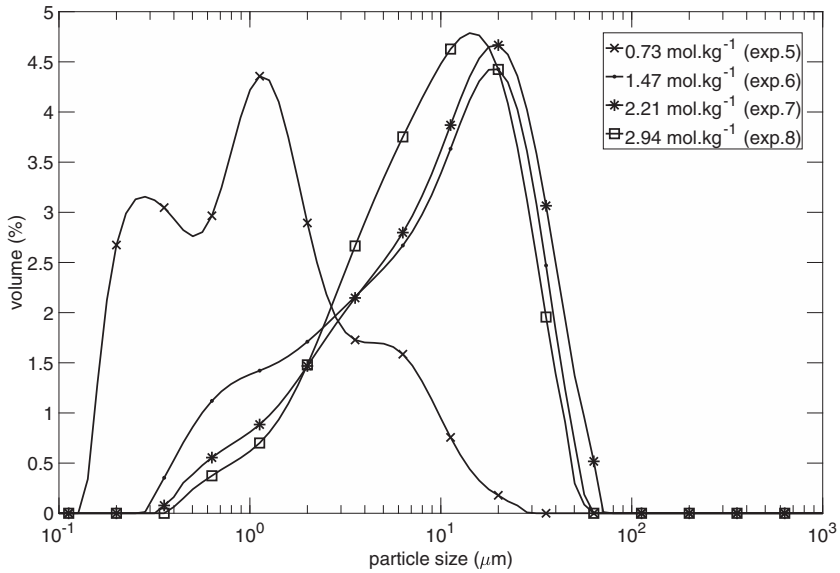


Fig. 10. Effects of initial reactants molalities on the particle-size distribution, during experiments with ultrasound (34.5 W).

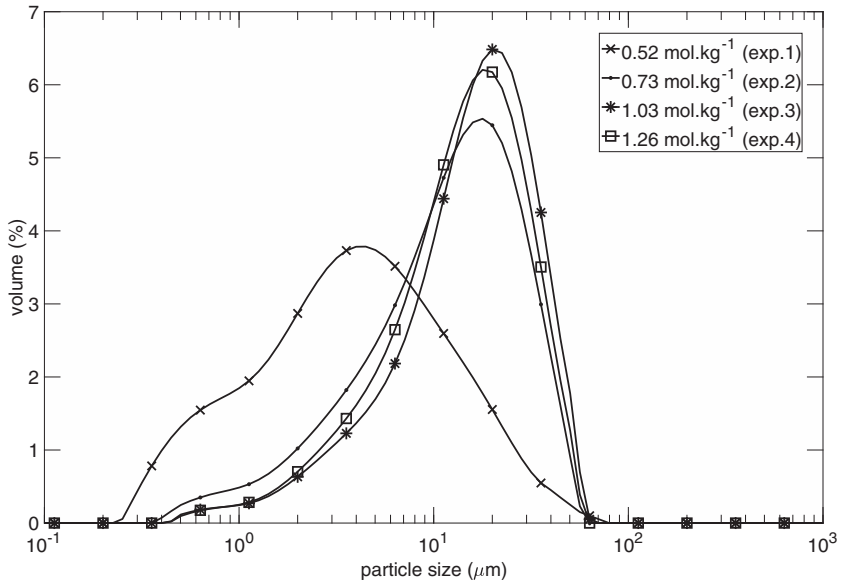


Fig. 11. Effects of initial reactants molalities on the particle-size distribution, during experiments without ultrasound.

Eq. (15) enables to determine r_{Nv}:

$$r_{Nv} = \frac{m_{v,2} m_{v,0}^2}{2\tau m_{v,1}^2} \tag{20}$$

5. Results and discussion

5.1. Size distribution and pH of suspension

Fig. 4 shows particle-size distributions at the exit of the mixing system (system 1) and at the exit of the tube connecting the mixing system and the stirred vessel (system 2). Both distributions are identical. Moreover, the pH of the suspension is almost identical in two locations for system 1 (the pH is 10.06) and for the system 2 (the pH is 10.10). Therefore no phenomenon occurs inside the tube. Nucleation, growth and agglomeration phenomena take place inside the mixing system. To calculate nucleation and growth rates and agglomeration kernel, particle-size distributions at the exit of the tube (system 2) and the mixing system volume (system 1) are considered.

Fig. 5 shows temporal particle-size distribution evolution for every experiment. Suspension sampling times are higher than 15 times the residence time τ. Apart from experiments 8 and 10 (Fig. 5 sub-plots h and j), particle-size distributions are stable, so the system is stationary.

For readability, the labels of axis are not written on Figures. The x-axis represents the size in μm and the y-axis the percentage volume of particles. (sub-plots a, b, …, m correspond to experiments 1, 2, …, 13 respectively).

5.2. Speciation calculations

Table 4 presents results of speciation calculations that were made for each experiment in the mixing system. pH^{exp} is the experimental pH. For two assumptions, calculated pH, pH^{calc}, supersaturation ratios, S, and moles numbers, n, are given. Results corresponding to the kept

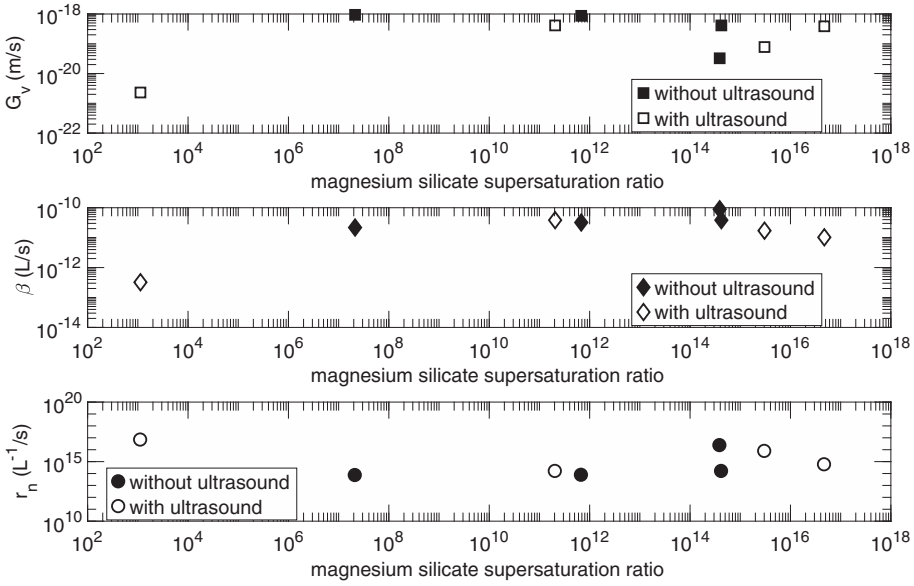


Fig. 12. Nucleation and growth rates and agglomeration kernel versus magnesium silicate supersaturation ratio and the use of ultrasound.

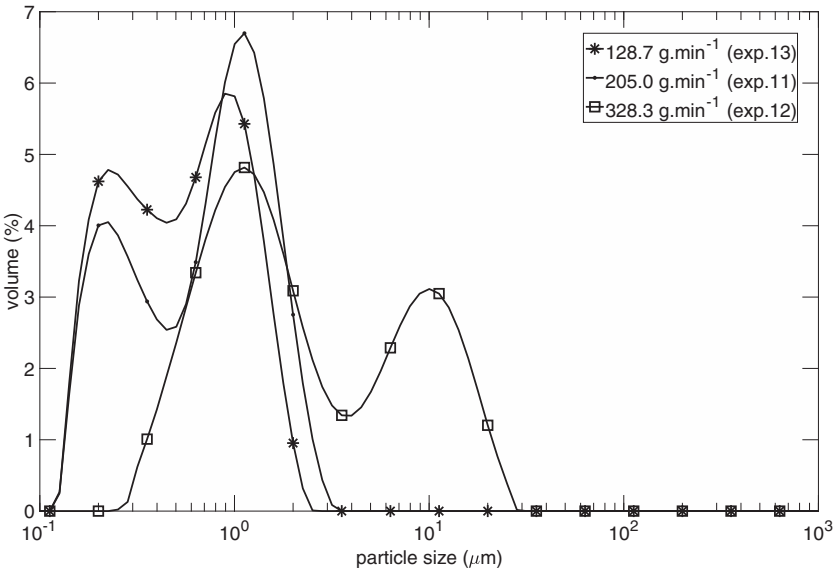


Fig. 13. Effects of reactants flow rate on the particle-size distribution. ([$MgCl_2$, $6H_2O$] = 0.73 mol·kg^{-1}, [HCl] = 1.00 mol·kg^{-1}, P_{US} = 34.5 W)

hypothesis are in bold characters. Magnesium silicate is represented by the subscript 1 whereas silica is represented by the subscript 2.

According to speciation calculations, in the mixing system, amorphous magnesium silicate would precipitate alone. It is supersaturated at the exit of the mixing system so its precipitation would end inside the vessel. With some operating conditions (hydrochloric acid excess, experiments 7 and 9 to 13), amorphous silica is supersaturated at the exit of the mixing system. Its precipitation kinetics would be slow so that it doesn't precipitate in the mixing system. However, it is difficult to determine if silica precipitates during or after reactants addition. At the end of the synthesis, with the highest hydrochloric acid excess, amorphous silica is slightly supersaturated. In the most of experiments, amorphous silica is at the equilibrium state at the end of the synthesis.

Operating conditions (reactants molalities, ultrasound power dissipation P_{US} and total reactants mass flow Q_M) of experiments are presented in Table 5. (See Table 6.)

5.3. Application of the population balance modelling

Volume moments are calculated from each particle-size distribution and medium volume moments are then calculated (see Appendix A).

Medium nucleation and growth rates and agglomeration kernel are determined from these medium volume moments. These medium values are those presented in Table 5 as function of magnesium silicate supersaturation ratio ($log(S)$).

5.3.1. Study of process parameters effects on crystallization rates

5.3.1.1. Ultrasound effects. Ultrasound power effects on particle-size distribution are studied from experiments 2 and 5. Both experiments were made with the same initial reactants molalities (Table 5). Fig. 6 shows effects of ultrasound on the particle-size distribution. Both distributions are very different. Particle sizes are smaller than 20 μm with ultrasound as against 70 μm without ultrasound. Ultrasound would thus appear to reduce particle sizes and prevent agglomerates from forming. This result has been already showed by Dodds et al. [7] about the ultrasound-assisted crystallization of $BaSO_4$, K_2SO_4, TiO_2 and sucrose particles.

Nucleation and growth rates and agglomeration kernel evolutions are represented in Fig. 7 versus initial reactants molalities and the use of ultrasound. Results of experiments 2 and 5 are circled on the figure. The ultrasound use causes the decrease of the growth rate and the agglomeration kernel, and the increase of the nucleation rate. Moreover, without considering initial reactants molalities, the ultrasound use generally causes the growth rate decrease and the nucleation rate increase.

Magnesium silicate supersaturation ratio increases when the precipitation operation occurs without ultrasound (Table 5).

Therefore ultrasound-assisted precipitation would enable to synthesize smaller particles and agglomerates by decreasing the supersaturation ratio, the growth rate and the agglomeration kernel and increasing the nucleation rate.

Ultrasound power effects on particle-size distribution can be studied from experiments 9, 10 and 11. These experiments were made with the same initial reactants molalities (Table 5). Particle-size distributions of these experiments are presented in Fig. 8. The increase of the ultrasound power enables particles and agglomerates sizes to decrease. This effect of ultrasound power has been already showed by Gatumel [10].

Fig. 9 shows effects of the ultrasound power on nucleation and growth rates and agglomeration kernel. When the ultrasound power increases, the nucleation rate firstly increases and then seems to decrease. This result has been formerly found by Gatumel [10]. The growth rate decreases and the agglomeration kernel decreases from 34.5 W.

On the other hand, magnesium silicate supersaturation ratio is not affected by the ultrasound power (Table 5).

The increase of ultrasound power would cause a decrease of the growth rate and the agglomeration kernel and an increase of the nucleation rate. But this increase is limited. From some ultrasound power value, the nucleation rate doesn't increase any more. These effects would explain the decrease of particles and agglomerates sizes as a result of the ultrasound power increase.

5.3.1.2. Initial reactants molalities effects. Effects of initial reactants molalities on the particle-size distribution can be studied from experiments 5 to 8 when the precipitation is ultrasound-assisted and from experiments 1 to 4 when the precipitation is not ultrasound-assisted.

Particle-size distributions of experiments 5 to 8 (ultrasound-assisted precipitation) are presented in Fig. 10. In this range of initial reactant molalities, particle-size distribution is strongly influenced.

Between [$MgCl_2$, $6H_2O$] = 0.73 mol·kg^{-1} and [$MgCl_2$, $6H_2O$] = 1.47 mol·kg^{-1}, distribution clearly shifts towards large sizes. Over 1.47 mol·kg^{-1}, particle-size distribution does not vary a lot. These results have been observed with other solids, such as strontium molybdate by Sohnel [15] and Dos Santos Nicolau Esteves Cameirao [3].

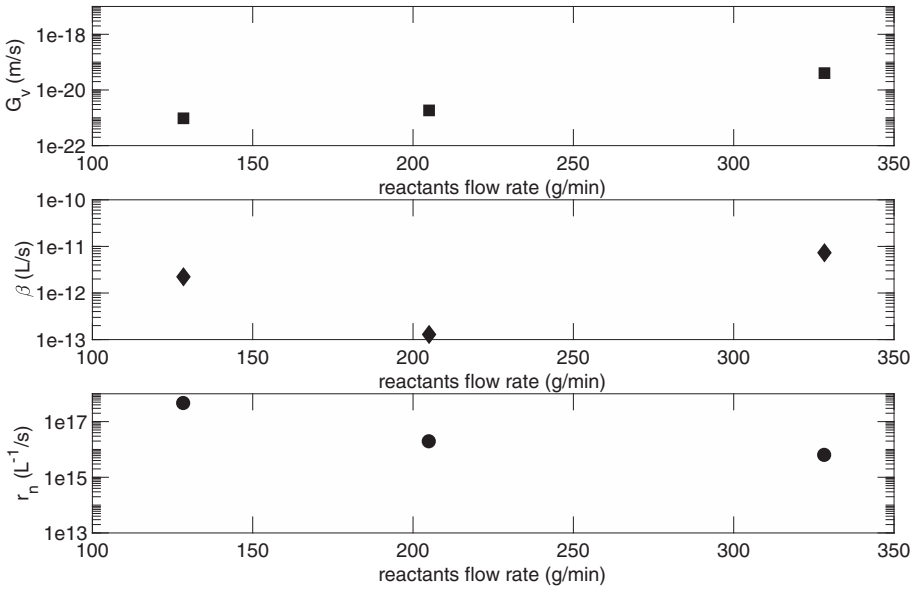


Fig. 14. Nucleation and growth rates and agglomeration kernel versus reactants flow rate.

Similar results are observed from experiments 1 to 4 (no-assisted precipitation) (Fig. 11). An effect of initial reactants molalities on particle-size distribution is observed between 0.52 and 0.73 mol·kg^{-1}: particles and agglomerates sizes decrease when molalities decrease. Up to 0.73 mol·kg^{-1}, the particle-size distribution doesn't vary any more. The molality from which the size distribution doesn't vary seems to be a function of the ultrasound power.

In Table 5, we can observe magnesium silicate supersaturation ratio decreases when initial reactants molalities increase, when the precipitation is not ultrasound-assisted. Moreover, when this supersaturation ratio increases, the nucleation rate and the agglomeration kernel increase too, whereas the growth rate decreases (Fig. 12).

Concerning the ultrasound-assisted precipitation (experiments 5 to 8), magnesium silicate supersaturation ratio conversely varies: it increases when initial reactants molalities increase. When this supersaturation ratio increases, the growth rate and the agglomeration kernel increase, whereas the nucleation rate decreases. This evolution of the nucleation rate is the opposite of the one that is usually observed. Indeed, the nucleation rate generally increases when the supersaturation ratio increases, as the following equation shows it [16]:

$$J_{sec} = k m_j^j S^b \tag{21}$$

with k a coefficient, m_j the ith order volume moment and S the supersaturation ratio.

In this study, we consider the secondary nucleation rate J_{sec} because the system is continuous and magnesium silicate particles are already formed in the suspension.

To explain the observed nucleation rate evolution, we suppose the global nucleation rate J_{sec} is made up of two elements: the secondary nucleation rate J_{sec}^{noUS} and a nucleation rate that leads to ultrasound J_{sec}^{US}:

$$J = J_{sec} + J_{US} \tag{22}$$

At high supersaturation values (higher than 10^{10} in this study) and at high solid concentration (between 0.0639 and 0.1145 kg·L^{-1}), we suppose the acoustic wave is weaken by the solid. Ultrasound effect would be inhibited because solid concentration is too high. The leading component of the global nucleation rate would be the secondary nucleation rate J_{sec}. The nucleation rate due to ultrasound would be negligible.

On the other hand, at low supersaturation values ($10^{3.05}$ in this study), the solid concentration is low too (0.0408 kg·L^{-1}). Ultrasound effect would not be inhibited, so the nucleation rate due to ultrasound J_{US} would be leading.

So we suppose that, if the acoustic wave was not weaken by the solid in the suspension, the global nucleation rate J would be higher, because the nucleation rate due to ultrasound J_{US} would be higher. If these hypothesis were true, the global nucleation rate would increase when the supersaturation increases, that would agree with works of other authors.

5.3.1.3. Reactants flow rate effects. Experiments 11 to 13 enable to study effects of reactants flow rate on the particle-size distribution. Fig. 13 represents particle-size distributions of these three experiments. When reactants flow rate decrease from 328.3 g·min^{-1} to 205.0 g·min^{-1}, the distribution shifts towards fine particles. When reactants flow rate decrease from 205.0 to 128.4 g·min^{-1}, the distribution width slightly changes but proportions of both particles populations change. Large particles population proportion (sizes about 1 μm) decreases whereas fine particles population proportion increases (sizes about 220 nm).

Fig. 14 shows nucleation and growth rates and agglomeration kernel versus reactants flow rates. The comparison of results from experiments made with 328.3 and 205.0 g·min^{-1} enables to observe that the growth rate and the agglomeration kernel decrease when reactants flow rate decreases. The decrease of the growth rate has been already observed by Franke [8] and Zauner and Jones [18] with the precipitation of calcium carbonate and calcium oxalate. On the other hand, the nucleation rate slightly varies. So the decrease of particles and agglomerates sizes, when reactants flow rates decrease, is due to the decrease of the growth rate and agglomeration kernel.

When reactants flow rates more decrease (from 205.0 to 128.4 g·min^{-1}), the nucleation rate and the agglomeration kernel increase. The growth rate doesn't change.

Moreover amorphous magnesium silicate supersaturation ratio isn't affected by reactants flow rates (Table 5).

6. Conclusions

Whatever process parameters, amorphous magnesium silicate would precipitate alone in the mixing system. It is supersaturated at the exit of the mixing system so its precipitation would end inside the vessel. An excess of hydrochloric acid causes the precipitation of amorphous silica inside the vessel. Even if it is slightly supersaturated at the

exit of the mixing system, we suppose its precipitation kinetics to be slow so silica precipitation would occur inside the vessel.

When the precipitation is ultrasound-assisted, the decrease of particles and agglomerates sizes would be due to the increase of the nucleation rate and the decrease of the growth rate and agglomeration kernel. These effects would be intensified by the increase of the ultrasound power dissipation. However, the increase of the nucleation rate would be limited: from some ultrasound power dissipation, it wouldn't increase any more. Moreover amorphous magnesium silicate supersaturation ratio would be influenced by the ultrasound use but not by the increase of the ultrasound power dissipation.

Particles and agglomerates sizes also decrease when initial reactants molalities decrease. Two opposite effects of molalities on the amorphous magnesium silicate supersaturation ratio are observed, depending on the use of ultrasound. If the precipitation is ultrasound-assisted, ultrasound effectiveness would be inhibited when solid concentration increases. The decrease of initial reactants molalities would cause the increase of the nucleation and the decrease of the growth rate and agglomeration kernel, that would explain the decrease of particles and agglomerates sizes.

Particles and agglomerates sizes finally decrease when reactants flow rate decreases. This effect would be due to the decrease of the nucleation rate and agglomeration kernel.

Acknowledgements

The authors acknowledge the Agence Nationale de la Recherche for the financial support of ANR-09-MAPR-0017 project. The authors also thank Ms. M.-A. Piquemal, Ms. H. Leroy and Ms. J. Ferret of Imerys Talc for XRF analyses.

Appendix A. Particles population density calculation

Before calculating nucleation and growth rates and agglomeration kernel, volume moments must be calculated. The three moments are calculated using the inner rectangles method. The particle-size distribution is divided into particles sizes classes. Every class i contains particles whose size is included in the interval $[L_i; L_i + dL_i]$ and whose volume is included in the interval $[V_i; V_i + dV_i]$. The whole of classes covers the sizes range between 0.02 μm and 2 mm. The size analysis gives the volume fraction $\%_{vol,\,i}$ of particles of every sizes class i. The particles population density $n_{v,\,i}$ is calculated for every sizes class i.

The particle volume V_i is written:

$$V_i = \phi_v L_i^3 \tag{A.1}$$

with ϕ_v the volume form factor (equal to $\frac{\Pi}{6}$ for spherical particles).

$\overline{V}_i$ is the medium volume of the class i:

$$\overline{V}_i = \frac{V_{i+1} + V_i}{2} \tag{A.2}$$

ΔV_i is the width of the class i:

$$\Delta V_i = V_{i+1} - V_i \tag{A.3}$$

The particles population density of the class i, $n_{v,\,i}$, is calculated from the following equation:

$$n_{v,i} = \frac{\%_{vol,i} M_T}{\rho \overline{V}_i \Delta V_i} \tag{A.4}$$

with M_T the mass concentration of particles in the suspension ($kg \cdot L^{-1}$) that is calculated from the following equation:

$$M_T = \frac{1}{\frac{m_{susp}}{\rho_{H_2O} n_{solid} M_{solid}} + \left(\frac{1}{\rho_{solid}} - \frac{1}{\rho_{H_2O}}\right)} \tag{A.5}$$

with m_{susp} the suspension mass (kg), ρ_{H_2O} and ρ_{solid} densities of water and solid ($kg \cdot m^{-3}$), M_{solid} the solid molar mass ($kg \cdot mol^{-1}$) and n_{solid} the solid moles number (mol) that is calculated using the computer software PHREEQC [6] at the exit of mixing system.

The density of the suspension is calculated from the following equation:

$$\rho_{susp} = \frac{\rho_{solid} \rho_{H_2O}}{w_{solid} \rho_{H_2O} + (1 - w_{solid}) \rho_{solid}} \tag{A.6}$$

with $w_{solid} = \frac{n_{solid} M_{solid}}{m_{susp}}$.

A.1. Volume moments calculation

The i^{th} order volume moment $m_{v,\,j}$ is calculated from the following equation:

$$m_{v,j} = \int_0^\infty n_v V^j dV \tag{A.7}$$

As a result, the 0^{th}, 1^{th} and 2^{th} order volume moments are:

$$m_{v,0} = \sum_i n_{v,i} \Delta V_i \tag{A.8}$$

$$m_{v,1} = \sum_i n_{v,i} \Delta V_i V_i \tag{A.9}$$

$$m_{v,2} = \sum_i n_{v,i} \Delta V_i V_i^2 \tag{A.10}$$

Appendix B. Electro-neutrality equation

$$\begin{aligned}&[OH^-] + [Cl^-] + \left[H_3SiO_4^-\right] \\ &\quad + 2\left[H_2SiO_4^{2-}\right] - [H^+] - [Na^+] - 2\left[Mg^{2+}\right] - [MgOH^+] = 0\end{aligned} \tag{B.1}$$

with $[i]$, the molality of species i in solution (mol/kg water).

B.1. Molar balance on silicon

$$\begin{aligned}n_{Si,0} &= [Si]_{solution} * m_{water} + 4n_{Si_4Mg_3O_{11},5H_2O} + n_{SiO_2} \\ &= \left([H_4SiO_4] + \left[H_3SiO_4^-\right] + \left[H_2SiO_4^{2-}\right]\right) * m_{water} \\ &\quad + 4n_{Si_4Mg_3O_{11},5H_2O} + n_{SiO_2}\end{aligned} \tag{B.2}$$

with m_{water}, the mass of water (kg). $n_{Si_4Mg_3O_{11},\,5H_2O}$ and n_{SiO_2} represent respectively the moles number of amorphous magnesium silicate and amorphous silica.

B.2. Molar balance on magnesium

$$\begin{aligned}n_{Mg,0} &= n_{Mg,solution} + n_{Mg,solide} \\ &= m_{water}\left(\left[Mg^{2+}\right] + [MgOH^+]\right) + 3n_{Si_4Mg_3O_{11},5H_2O}\end{aligned} \tag{B.3}$$

B.3. Molar balance on sodium

$$n_{Na,0} = \left[Na^+\right] m_{water} \tag{B.4}$$

B.4. Molar balance on oxygen

$$n_{O,0} - 16 n_{Si_4Mg_3O_{11},5H_2O} - 2 n_{SiO_2} - m_{water}\left(\left[OH^-\right] + \left[MgOH^+\right] + 4\left(\left[H_4SiO_4\right] + \left[H_3SiO_4^-\right] + \left[H_2SiO_4^{2-}\right]\right)\right) = 0 \tag{B.5}$$

B.5. Molar balance on hydrogen balance

$$n_{H,0} - 10 n_{Si_4Mg_3O_{11},5H_2O} - m_{water}\left(\left[OH^-\right] + \left[H^+\right] + \left[MgOH^+\right] + 4\left[H_4SiO_4\right] + 3\left[H_3SiO_4^-\right] + 2\left[H_2SiO_4^{2-}\right]\right) = 0 \tag{B.6}$$

B.6. Ionic strength of the solution

$$I = 0,5\sum_i (z_i)^2 [i] = 0,5\left(\left[OH^-\right] + \left[H^+\right] + \left[Cl^-\right] + 4\left[Mg^{2+}\right] + \left[MgOH^+\right] + \left[Na^+\right] + \left[H_3SiO_4^-\right] + 4\left[H_2SiO_4^{2-}\right]\right) \tag{B.7}$$

B.7. Activity of water [Garrels and Christ [9]]

$$a_{water} = 1 - 0.017\sum_i^N [i] \tag{B.8}$$

The two solids are assumed to be pure, therefore their activities $a_{Si_4Mg_3O_{11},nH_2O}$ and a_{SiO_2} are equal to 1.

References

[1] F. Baillon, F. Espitalier, C. Cogné, R. Peczalski, O. Louisnard, Chapter 28: Crystallization and freezing processes assisted by power ultrasound, in: Juan A. Gallego-Juárez, Karl Graff (Eds.),Power Ultrasonics (1st Edition): Applications of High-Intensity Ul-trasound, Woodhead publishing series in electronic and optical materials, , 2015.

[2] A.J. Bard, R. Parsons, J. Jordan, IUPAC, Marcel Dekker Inc., New York, 1985.

[3] A.A. Dos Santos Nicolau Esteves Cameirao, Étude expérimentale et modélisation d'une précipitation avec agglomération entre cristaux de morphologies différentes: application au molybdate de strontium, Thèse de l'Institut National Polytechnique de Toulouse, 2007.

[4] S.R. Charlton, D.L. Parkhurst, Modules based on the geochemical model PHREEQC for use in scripting and programming languages, Comput. Geosci. 37 (2011) 1653–1663.

[5] F. Ciesielczyk, A. Krysztafkiewicz, K. Bula, T. Jesionowski, Evaluation of synthetic magnesium silicate as a new polymer filler, Compos. Interfaces 17 (2010) 481–494.

[6] M. Dietemann, F. Baillon, F. Espitalier, R. Calvet, P. Accart, S. Del Confetto, M. Greenhill-Hooper, Evaluation of the physico-chemical properties of an amorphous magnesium silicate synthesized by an ultrasound-assisted precipitation, Chem. Eng. J. 215 (2013) 658–670.

[7] J. Dodds, F. Espitalier, O. Louisnard, R. Grossier, R. David, M. Hassoun, F. Baillon, C. Gatumel, N. Lyczko, The effect of ultrasound on crystallisation-precipitation processes: some examples and a new segregation model, Part. Part. Syst. Charact. 24 (2007) 18–28.

[8] J. Franke, A. Mersmann, The influence of the operational conditions on the precipitation process, Chem. Eng. Sci. 50 (1995) 1737–1753.

[9] R. Garrels, J. Christ, Solution, Minerals, and Equilibria, 1965.

[10] C. Gatumel, Précipitation du sulfate de baryum sous ultrasons: effets sur le micromélange et sur la nucléation, Thèse de l'Institut National Polytechnique de Toulouse, 1997.

[11] H.M. Hulburt, S. Katz, Some problems in particle technology: a statistical mechanical formulation, Chem. Eng. Sci. 19 (1964) 555–574.

[12] F. Martin, Le talc: un minéral idéal ? Habilitation à Diriger des Recherches, Université Toulouse III, Paul Sabatier, 1999.

[13] F. Martin, J. Ferret, C. Lèbre, S. Petit, O. Grauby, J.-P. Bonino, D. Arseguel, A. Decarreau, Procédé de préparation d'une composition de talc synthétique à partir d'une composition de kérolites, Brevet d'invention français FR2903682 - A1 - 2006, 2006.

[15] O. Sohnel, J.W. Mullin, A.G. Jones, Crystallization and agglomeration kinetics in the batch precipitation of strontium molybdate, Ind. Eng. Chem. Res. 27 (1988) 1721–1728.

[16] N.S. Tavare, Industrial Crystallization: Process Simulation Analysis and Design, Plenum Press, 1995.

[17] Tufar, Talc, 2000.

[18] R. Zauner, A. Jones, Mixing effects on product particle characteristics from semi-batch crystal precipitation, Chem. Eng. Res. Des. 78 (2000) 894–902.